Supplementary Information

Effects of Catalyst Morphology on Oxygen Defects at Ni-CeO_2 Interfaces for CO_2 Methanation

Samiha Bhat[1], Miguel Sepúlveda-Pagán[2], Justin Borrero-Negrón[2], Jesús E. Meléndez-Gil[2],

Eranda Nikolla[1*], Yomaira J. Pagán-Torres[2*]

[1]Department of Chemical Engineering, University of Michigan,

Ann Arbor, MI, United States

[2]Department of Chemical Engineering, University of Puerto Rico-Mayagüez Campus,

Mayagüez, PR, United States

*Corresponding authors: erandan@umich.edu, yomairaj.pagan@upr.edu

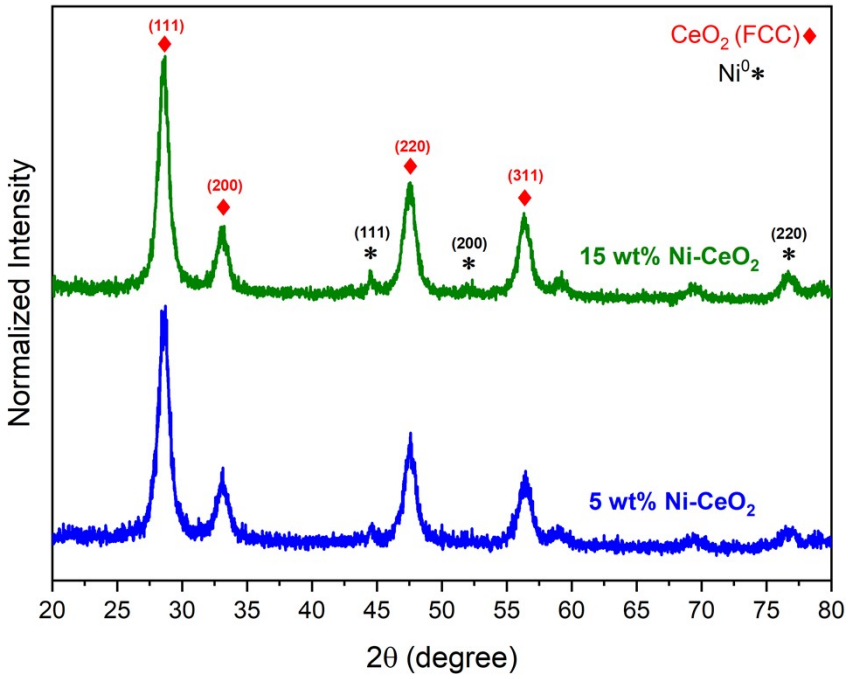

Figure S1. XRD patterns of 5 wt% and 15 wt% Ni-CeO_2 catalysts showing the increase in the Ni (111) peak intensity as a function of Ni loading.

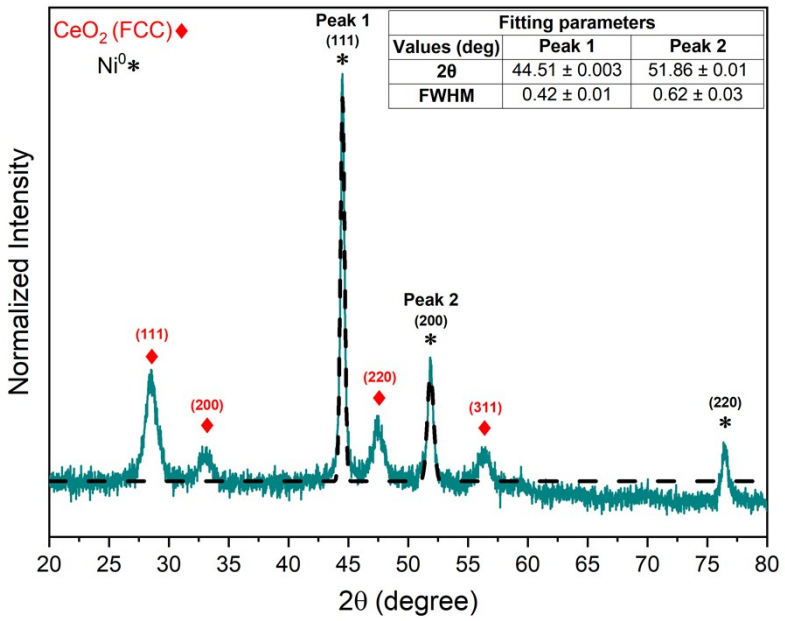

Figure S2. XRD pattern for the 60 wt% Ni-CeO_2 catalyst along with the fitting parameters (inset table) obtained for the Ni(111) and Ni(200) peaks post Gaussian peak fitting.

The Ni crystallite size was determined by averaging the absolute crystallite sizes (D) obtained from the (111) and (200) Ni peaks using the Scherrer equation –

$$D\ (nm) = \frac{k\,\lambda}{\beta \cos\theta}$$

The shape factor or (k) and X-ray wavelength (λ) were assumed to be 0.9 and 0.15 nm, respectively. The full width half maximum (FWHM, β) and diffraction angle (θ) in radians were obtained from Gaussian fitting of the diffraction peaks and are presented in the inset table in Fig S2.

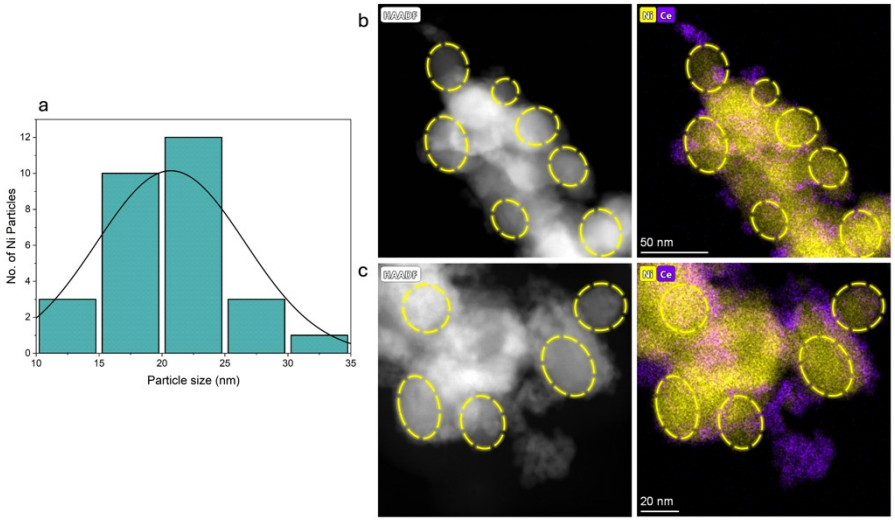

Figure S3. (a) Size distribution histogram for 60wt% Ni-CeO_2 catalyst obtained by measuring 30 Ni NPs. (b, c) HAADF-STEM images along with EDS elemental mapping for 60 wt% Ni-CeO_2 catalyst outlining the Ni particles (yellow dashes) measured for particle size distribution.

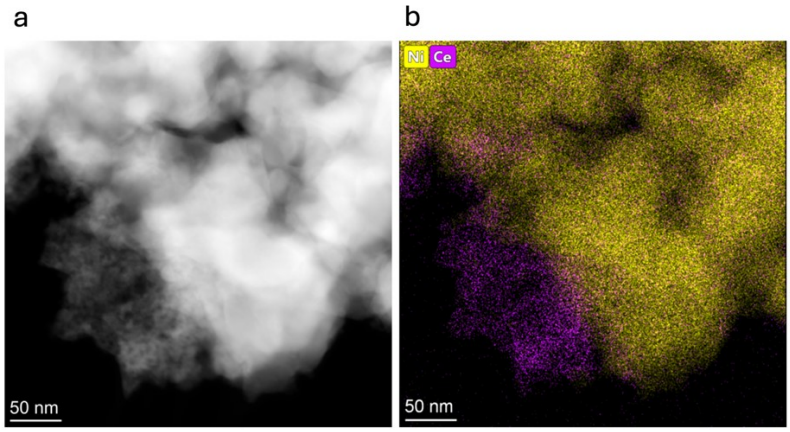

Figure S4. (a) HAADF-STEM image and (b) EDS elemental mapping of 40 wt% Ni-CeO_2 catalyst depicting an inverse catalytic structure.

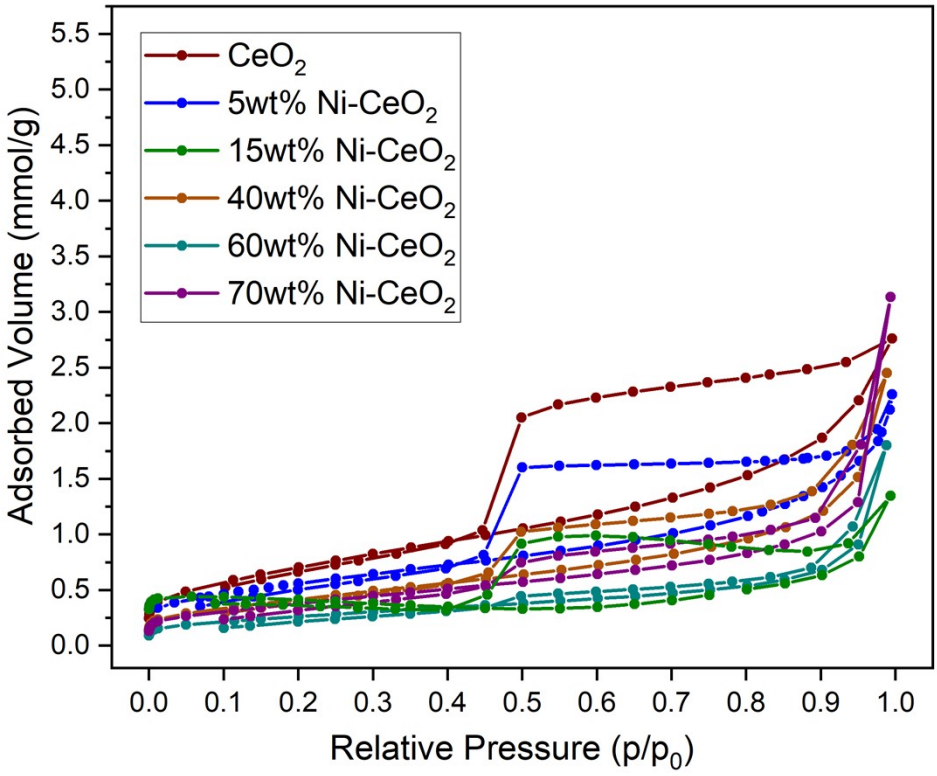

Figure S5. Nitrogen adsorption-desorption isotherms for X wt% Ni-CeO_2 catalysts (where X = 5, 15, 40, 60, 70).

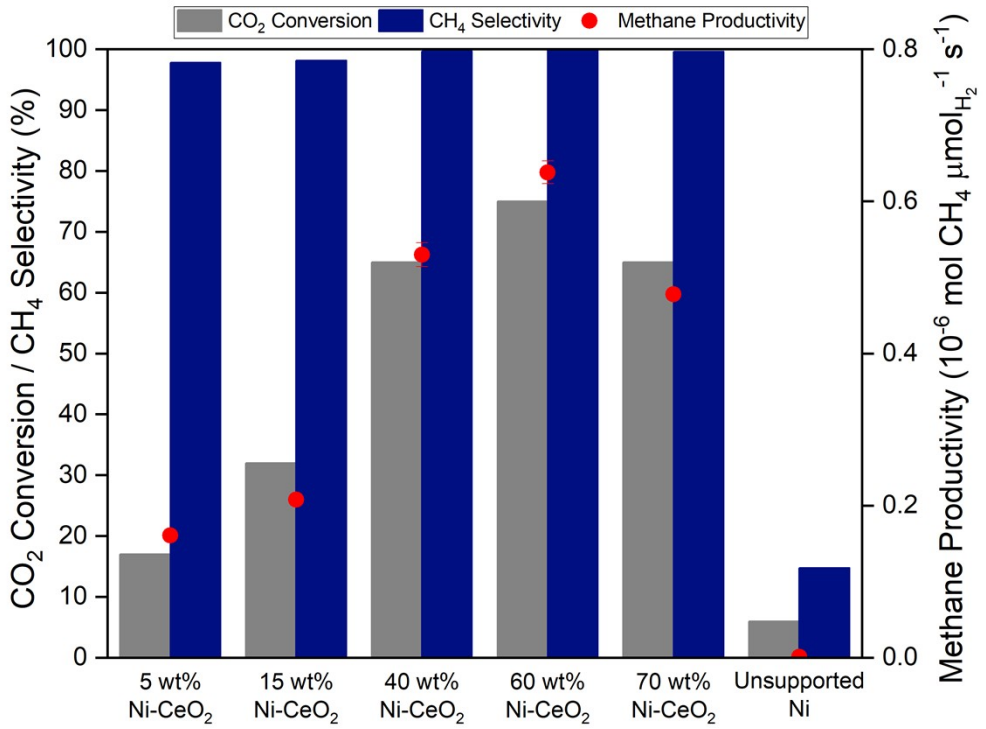

Figure S6. Catalytic performance for CO_2 methanation over X wt% Ni-CeO_2 catalysts (where X = 5, 15, 40, 60, 70) at 275°C. Methane productivity is normalized with respect to µmoles of H_2 adsorbed based on H_2 pulse chemisorption. Reaction conditions: P = 1 atm, GHSV = 15,000 mL g_{cat}^{-1} h^{-1}, T = 275°C, H_2/CO_2 = 4.

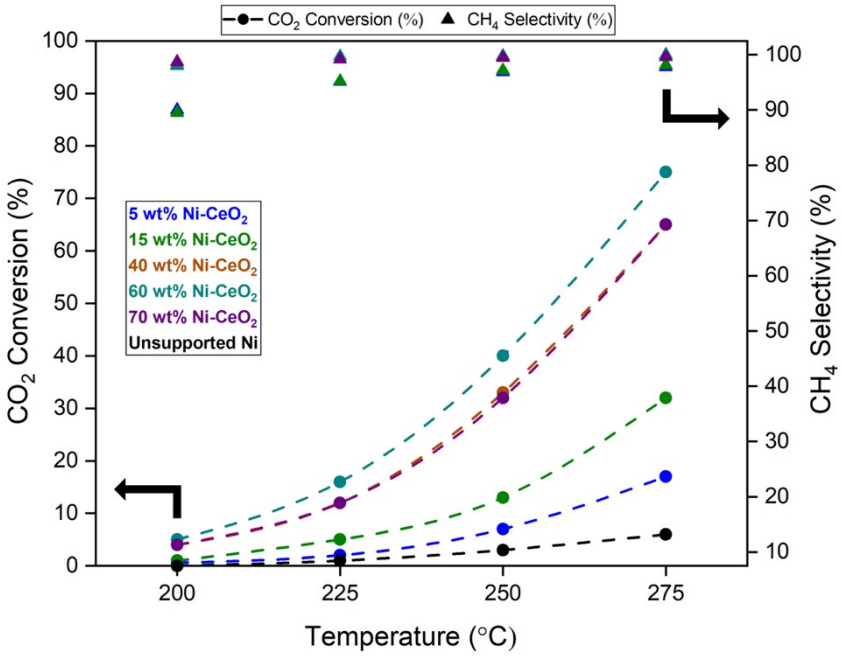

Figure S7. Catalytic performance of X wt% Ni-CeO_2 catalysts (where X = 5, 15, 40, 60, 70) in CO_2 methanation. Reaction conditions: P = 1 atm, GHSV = 15,000 mL g_{cat}^{-1} h^{-1}, H_2/CO_2 = 4, T = 200-275°C.

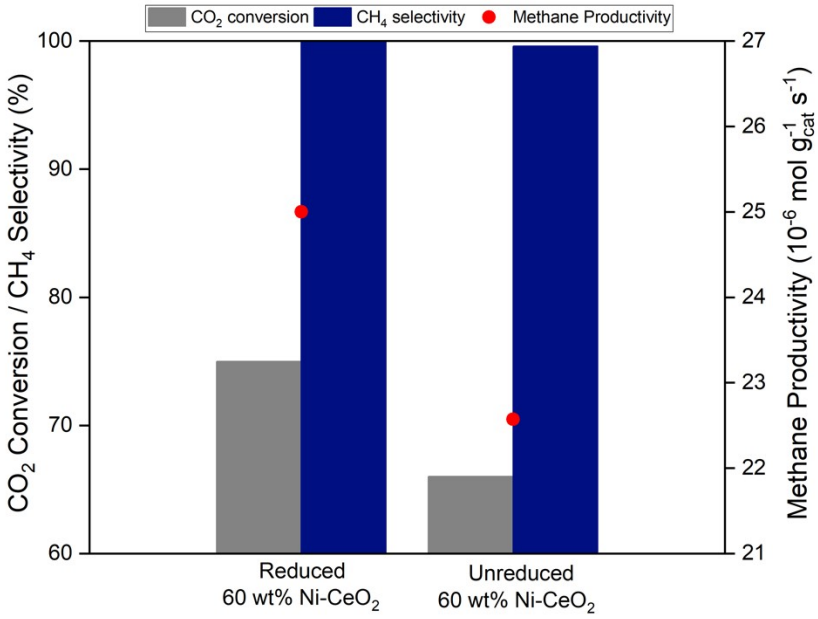

Figure S8. Catalytic performance of inverse 60 wt% Ni-CeO_2 catalyst reduced in-situ prior to catalytic testing at 425 °C (5°C/min ramp, 4 h hold) under a flow of H_2 at 40 mL/min and the unreduced catalyst post ex-situ calcination at 400 °C (5°C/min ramp, 3 h hold). Reaction conditions: P = 1 atm, GHSV = 15,000 mL $g_{cat}^{-1}h^{-1}$, T = 275 °C, $H_2/CO_2 = 4$.

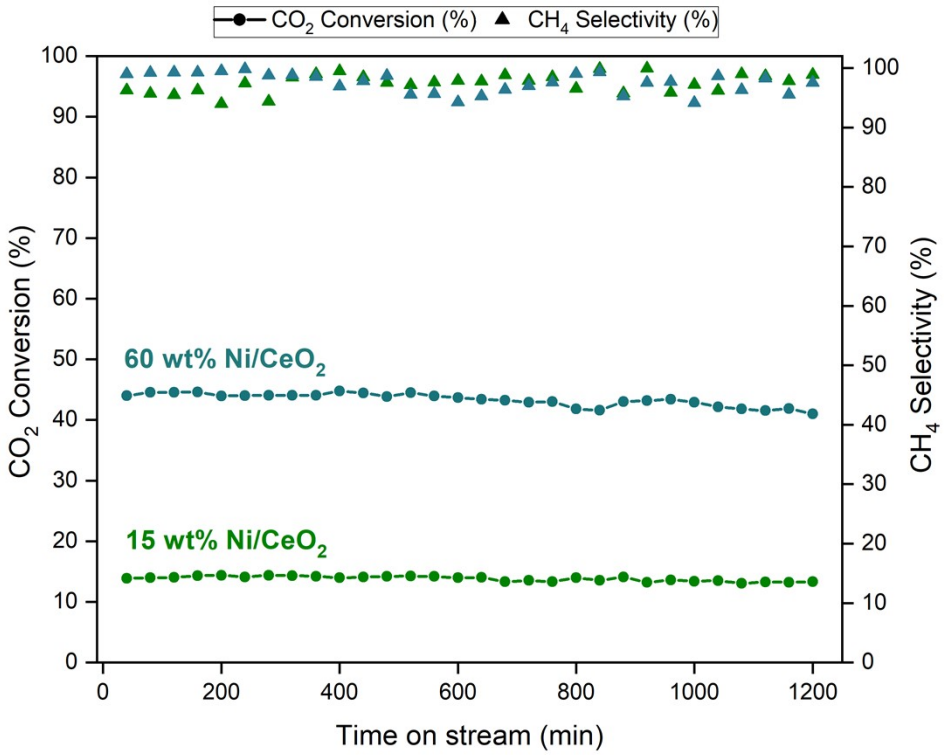

Figure S9. Stability test of the best performing inverse 60 wt% Ni-CeO_2 and supported 15 wt% Ni-CeO_2 catalyst. Reaction conditions: P = 1 atm, GHSV = 15,000 mL $g_{cat}^{-1}h^{-1}$, T = 250 °C, $H_2/CO_2 = 4$.

Table S1. Intensity ratios of D_1 and F_{2g} peaks obtained from Raman studies of Ni-CeO_2 catalysts.

Entries	**Catalyst**	**I_{D1}/I_{F2g}**
1	5 wt% Ni-CeO_2	0.29
2	15 wt% Ni-CeO_2	0.57
3	40 wt% Ni-CeO_2	0.64
4	60 wt% Ni-CeO_2	1.30
5	70 wt% Ni-CeO_2	0.96
6	60 wt% Ni 1 wt% Gd-CeO_2	1.16
7	60 wt% Ni 1 wt% La-CeO_2	1.58
8	60 wt% Ni 1 wt% Pr-CeO_2	1.90

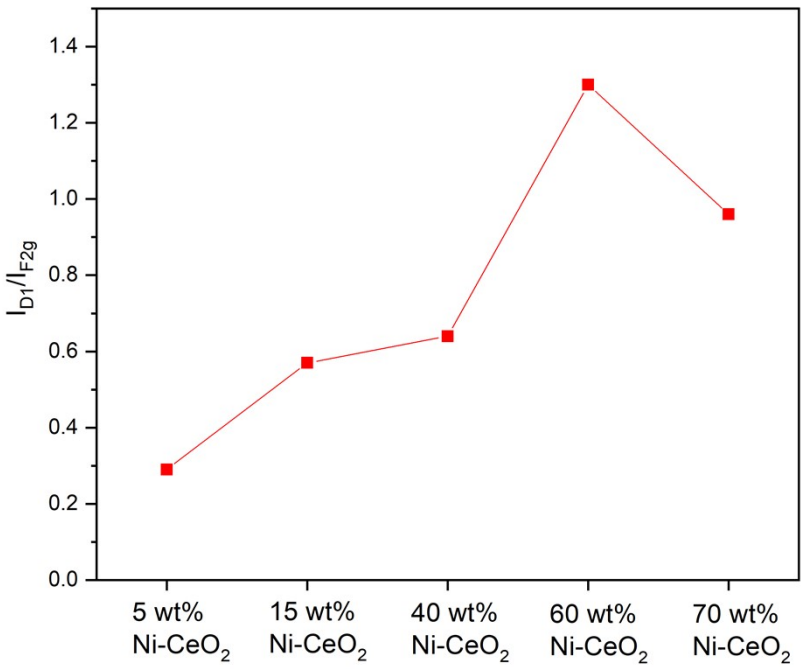

Figure S10. Intensity ratios of the Raman D_1 to F_{2g} bands (I_{D1}/I_{F2g}) as a function of Ni loading in Ni-CeO_2 catalysts.

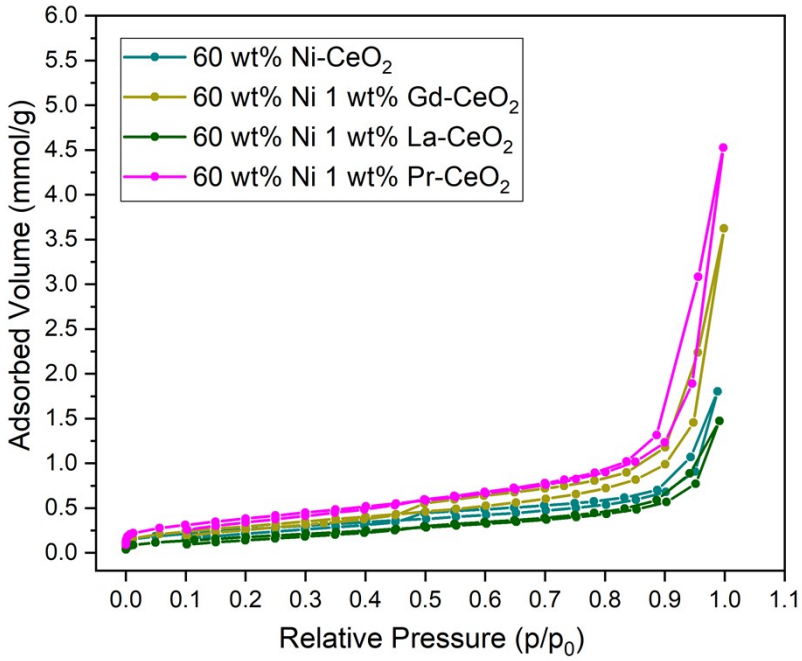

Figure S11. Nitrogen adsorption-desorption isotherms for 1 wt% Pr, La, or Gd doped 60 wt% Ni-CeO_2 and 60 wt% Ni-CeO_2 catalysts.

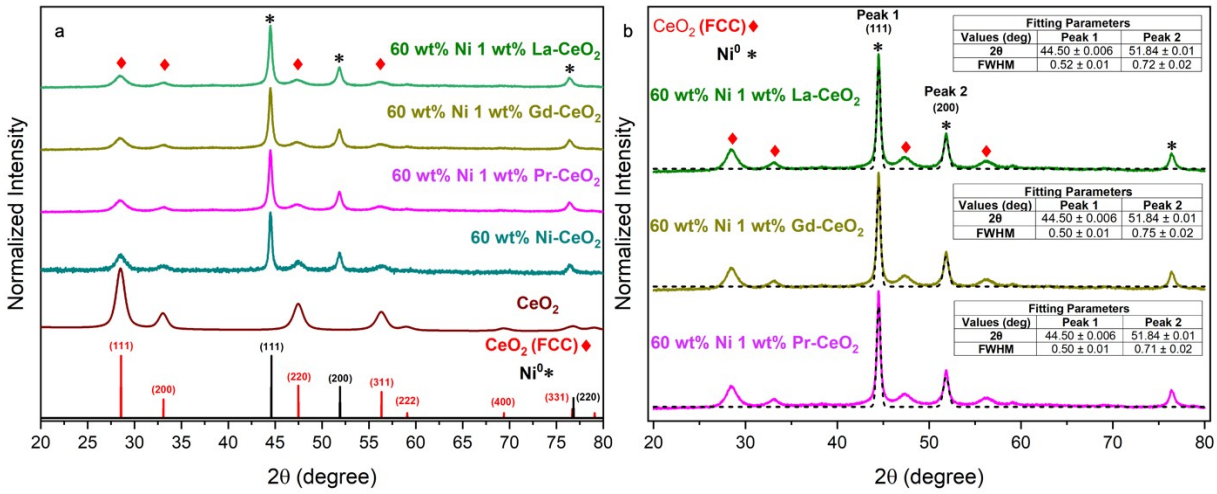

Figure S12. (a) XRD pattern of 60 wt% Ni-CeO_2, 1 wt% Pr, La, or Gd doped 60 wt% Ni-CeO_2, and CeO_2. (b) XRD pattern for the 1wt% Pr, La, and Gd doped 60 wt% Ni-CeO_2 catalyst along with the fitting parameters (inset tables) obtained for the Ni(111) and Ni(200) peaks post Gaussian peak fitting.

The Ni crystallite size was determined by averaging the absolute crystallite sizes (D) obtained from the (111) and (200) Ni peaks using the Scherrer equation –

$$D\ (nm) = \frac{k\,\lambda}{\beta \cos\theta}$$

The shape factor or (k) and X-ray wavelength (λ) were assumed to be 0.9 and 0.15 nm, respectively. The full width half maximum (FWHM, β) and diffraction angle (θ) in radians were obtained from Gaussian fitting of the diffraction peaks and are presented in the inset table in Fig S12.

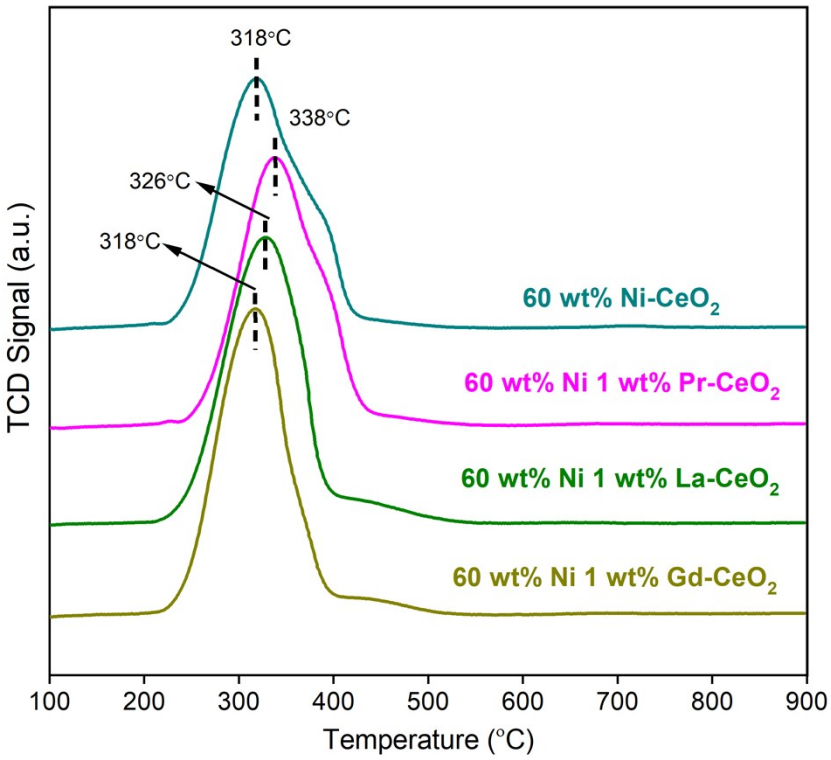

Figure S13. H_2-TPR profiles for 1 wt% Pr, La, or Gd doped 60 wt% Ni-CeO_2 and 60 wt% Ni-CeO_2.

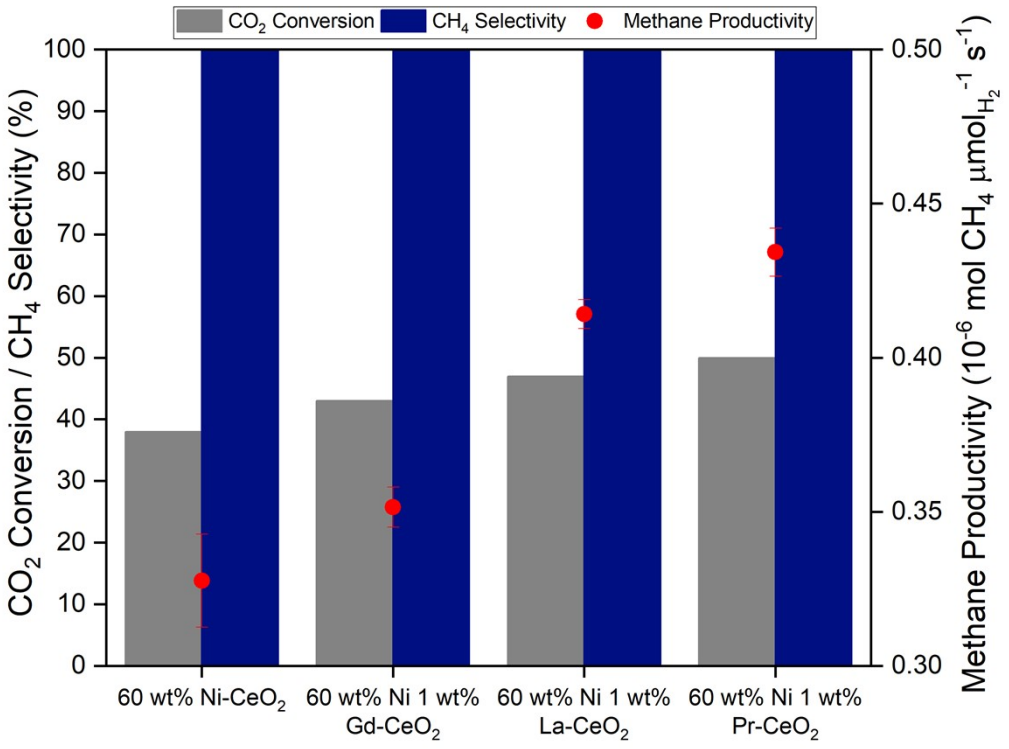

Figure S14. Catalytic performance for CO_2 methanation over 1 wt% Pr, La, or Gd doped 60 wt% Ni-CeO_2 and 60 wt% Ni-CeO_2 at 250°C. Methane productivity is normalized with respect to µmoles of H_2 adsorbed based on H_2 pulse chemisorption. Reaction conditions: P = 1 atm, GHSV = 15,000 mL g_{cat}^{-1} h^{-1}, T = 250°C, H_2/CO_2 = 4.

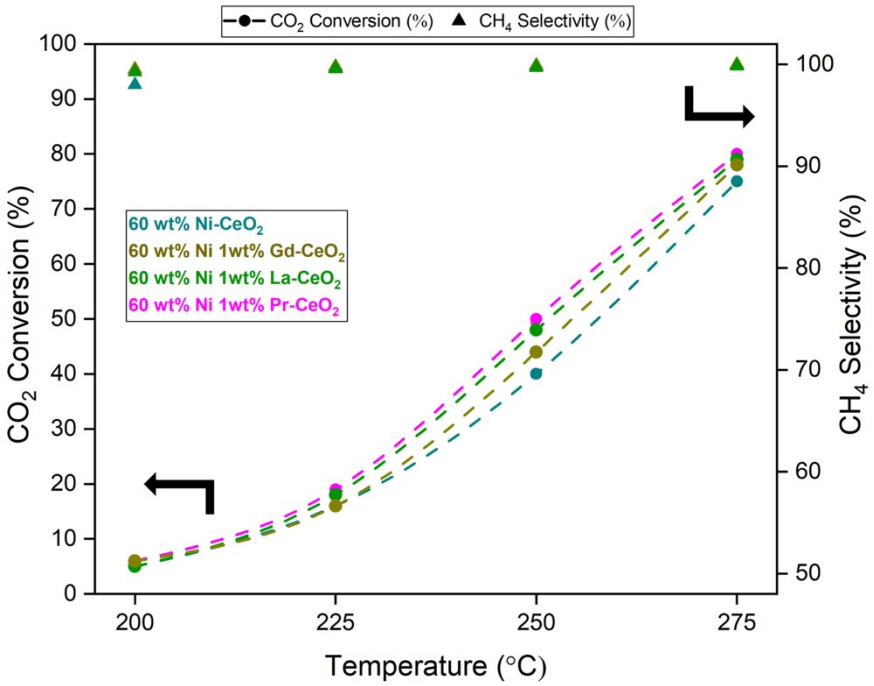

Figure S15. Catalytic performance of 1 wt% Pr, La, or Gd doped 60 wt% Ni-CeO_2 and 60 wt% Ni-CeO_2 in CO_2 methanation. Reaction conditions: P = 1 atm, GHSV = 15,000 mL g_{cat}^{-1} h^{-1}, H_2/CO_2 = 4, T = 200-275°C.

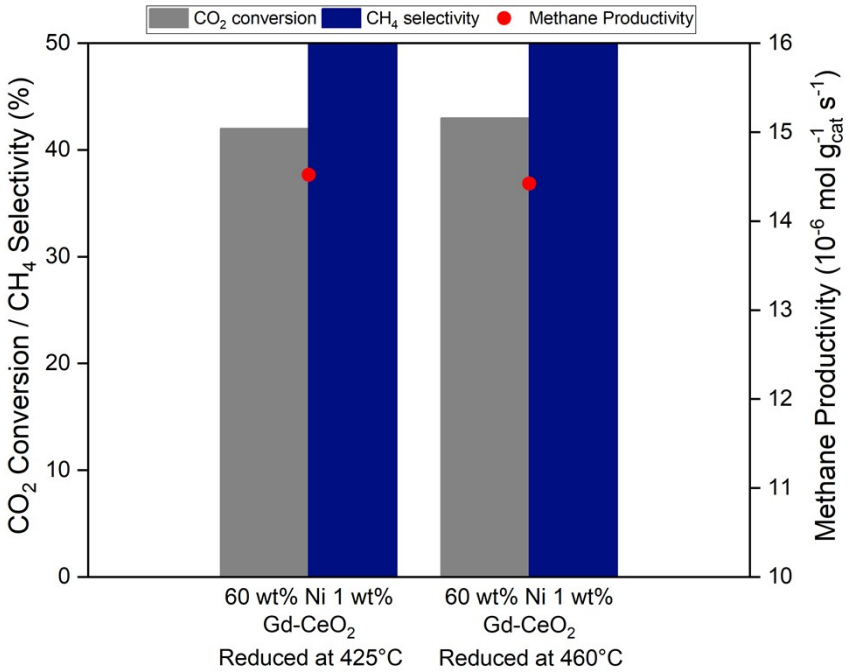

Figure S16. CO_2 conversion/CH_4 selectivity and methane productivity (secondary y-axis) of 60 wt% Ni 1 wt% Gd-CeO_2 reduced in situ at 425°C and 460°C (5°C/min ramp, 4 h hold) under a flow of H_2 at 40 mL/min prior to catalytic testing. Reaction conditions: P = 1 atm, GHSV = 15,000 mL $g_{cat}^{-1}h^{-1}$, T = 250 °C, $H_2/CO_2 = 4$.

The natural log of the Arrhenius equation was used to determine the apparent activation energy for methane formation as shown below:

$$\ln(k) = -\frac{E_A}{R}\left(\frac{1}{T}\right) + \ln(A)$$

Where k represents the reaction rate constant which scales with the rate of methane formation, A is the preexponential or frequency factor, E_A is the activation energy, R is the ideal gas constant (8.3145 J K^{-1} mol^{-1}) and T is the temperature.

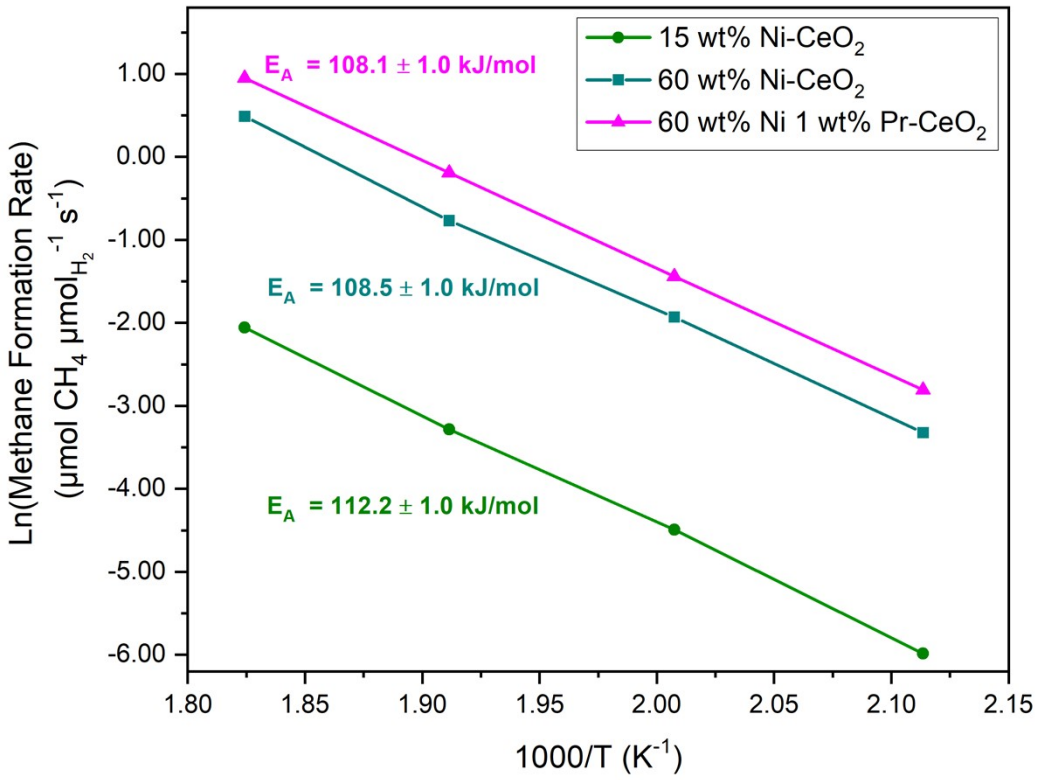

Figure S17. Arrhenius plot for 15 wt% Ni-CeO_2, 60 wt% Ni-CeO_2, and 60 wt% Ni 1 wt% Pr-CeO_2 catalysts.